Marine Structures 104 (2025) 103879

Contents lists available at ScienceDirect

Marine Structures

journal homepage: www.elsevier.com/locate/marstruc

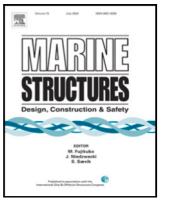

Simulated ice loads on a ship propeller and comparison with full-scale measurements

Jorrid Lund *, Lina Sapp, Jan Manuel Kubiczek, Angelo Mario Böhm, Franz von Bock und Polach

Institute for Ship Structural Design and Analysis (M-10), Hamburg University of Technology (TUHH), Am Schwarzenberg Campus 4 C, 21073 Hamburg, Germany

ARTICLE INFO

Keywords:
Propeller-ice interaction
Computational mechanics
Mohr-Columb nodal split
Floe-ice breaking
Mechanical properties of polar ice
Ice-load spectrum
Ships in ice

ABSTRACT

A methodology to better estimate the loads of ice acting on the propeller of a ship is developed. Based on measurements conducted in the North Pole region, an existing failure model for ice based on the Mohr–Coulomb nodal split approach is modified to better represent the lower strength of polar ice compared to laboratory ice. The modified material model for the sea ice is used to compute the propeller torque and a load spectrum for the propeller-ice interaction of the research ship *S.A. Agulhas II*. To this end, a floe-ice breaking simulation is used to estimate the size and shape of the ice cusps hitting the propeller of this ship. In the next step, a set of finite element simulations of the propeller-ice interaction utilizing the modified Mohr–Coulomb nodal split model is conducted. Based on this, the load spectrum is computed and compared with the measured torque on the propeller shaft of the *S.A. Agulhas II*. The successful reproduction shows the applicability of the approach to better estimate the loads exerted by the ice on the propeller.

1. Introduction

In recent years, maritime activities in the polar regions increased significantly [1][2,3, 38 f.]. The polar regions have been important for research and military ships for centuries. But in recent years, also commercial ships and tourism have frequented the polar region more. More ship traffic in the polar regions in floe-ice fields also leads to more collisions between sea ice and the ship propeller. It is shown by some incidents of ships operating in ice floe fields [4,5], that the propeller and the attached drive train are some of the most exposed and compromised components of a ship in these circumstances.

With ice melting due to climate change, the Arctic Ocean is also increasingly attractive for cargo ships [6, p. 35]. The Northeast Passage offers a much shorter route from northern Europe to many ports in East Asia [6, p. 44]. Additionally, it avoids the interference-prone and region of the Suez Canal. The projections of future developments of the Arctic ice coverage with even potential ice-free Arctic summers [7] might also offer transit options for ships with lighter ice classes. This could be exploited by larger cargo ships, decreasing significantly the costs and emissions caused by large cargo ships in the transport of goods.

Despite this, the operation of a ship operating in ice still poses many challenges [8]. The increased cost for a more robust ship operating in ice floe fields and the potential danger of a failure of components of a ship in these conditions pose problems for the operations of ships in ice. A failure of critical parts of a ship such as the propulsion system or the hull leads to an increased risk for the integrity of the environment and humans, but also financial losses for extraordinary maintenance.

* Corresponding author.
E-mail address: Jorrid.Lund@tuhh.de (J. Lund).

https://doi.org/10.1016/j.marstruc.2025.103879
Received 23 August 2024; Received in revised form 11 December 2024; Accepted 8 June 2025
Available online 3 July 2025

Table 1
Vessel specifications of the *S.A. Agulhas II*.

Ice class	PC 5
Length	134.2 m
Beam	21.7 m
Draft	7.65 m
No. of blades	4
n = speed (power at MCR)	$2.\bar{3}$ rps (4500 kW)
D = diameter	4.3 m
EAR = expanded blade area ratio	0.51
d = propeller hub diameter	1.32 m
$P_{0.7}$ = maximum propeller pitch at 0.7 R	5.15 m
$c_{0.7}$ = length of the blade chord at 0.7 R	1.105 m
$t_{0.7}$ = max thickness at 0.7 R	0.1 m

For safe and economically efficient operations of ships in ice conditions, an accurate estimation of the ice loads acting on the ship and its components is essential. The loads on the propeller affect not only the propeller blades, hub or shaft, but also any component attached, such as the bearings or even motors [9]. Consequently, it is essential to prove that occurring loads are below design loads or within acceptance criteria [10,11].

The accurate determination of the load on a ship propeller in such conditions is still a challenge due to the lack of direct measurements. First prominent work in the field was done by Veitch and Soininen [12,13]. Both utilized the Mohr–Coulomb failure criterion for the ice material definition. Veitch developed a detailed contact model for the prediction of thrust and torque including hydrodynamics and blocking, but comparisons with full-scale measurements still showed a significant under prediction of the occurring forces and torque [12]. The approach of Soininen is similar in scope, but different in method. Soininen [13] developed a contact model for propeller-ice interaction including hydrodynamic disturbance loads, but for the modelling an ice block of infinite mass is assumed. Furthermore, the ice properties have been represented by the compressive strength. The model was validated by measured blade bending moments as a function of changing angles of attacks, with some agreement, which Soininen [13] considered indicative. It is acknowledged that pioneering work is done by Wang [14] in model ice and numerical models exist [15] using this as validation. However, significant limitations already arise from the use of model ice, which has certain limitations and cannot be considered to provide scalable results in all aspects [16,17]. Several ice material models and methods exist as e.g. smoothed-particle hydrodynamics (SPH), peridynamics, the cohesion element method (CEM), and the discrete element method (DEM) [18]. The Mohr–Coulomb material model within the FEM framework is simple, physically interpretable, and has proven effective in multiple cases. In practice, the design of the propeller on a ship operating in ice conditions is performed on strongly simplified assumptions such as a constant pressure acting on the blade in different areas [11].

In order to bridge this gap, this paper aims to provide a framework and methodology, with which the loads acting on a ship propeller in ice conditions can be computed and assessed directly. With this framework, measurements conducted on the *S.A. Agulhas II* [19,20] are reproduced. This approach aims towards predicting loading with higher accuracy and loads that cannot be measured directly in operations such as lateral loads on the propeller and its impact on bearings [21]. This aims to support the development of a digital twin of a ship in ice conditions [9], which may ultimately be used to compute more accurate load spectra for fatigue life and potential maintenance planning for which currently still rule based approaches need to be employed [22].

In Section 3, broken floe ice patterns for the research ship *S.A. Agulhas II* are determined with a floe ice simulation approach which was introduced in [23]. In Section 4 a set of measurements of the compressive failure of sea ice conducted during an Arctic expedition is presented. These measurements are used in Section 5 to improve an existing ice model [24] based on the Mohr–Coulomb Nodal Split (MCNS) model. With the improved MCNS model, a set of explicit finite-element simulations is performed to simulate the interaction between the propeller of the *S.A. Agulhas II* and the broken ice floes computed in Section 3. With these simulations an ice-load spectrum for the *S.A. Agulhas II* is computed in and compared to the loads obtained based on measurements on the propeller shaft of the *S.A. Agulhas II*. At the end, the results are discussed in Section 8, and a Summary and Conclusion are given in Section 9.

The MCNS model has been previously validated under dynamic condition in a number of paper [25–27]. The model has also been validated on propeller model edges [18].

To the best of the author's knowledge, there are no previous works that present a simulation framework that combines the breaking of the ice at the bow of the ship and at the propeller blade, which is capable of reproducing the loads acting on a propeller blade due to sea ice.

2. Characteristics of S.A. Agulhas II

The *S.A. Agulhas II* is a South African Polar supply and research vessel. It has already been subjected to several research projects as it is here.

The water line hull shape is used for the ice-breaking simulations and the geometry of its propellers is used for the simulation of the propeller ice interaction. Geometric details and key parameters are found in Table 1.

The assigned ice class PC5 refers according to [10] to operations in medium first-year ice with old ice inclusions. Medium first-year ice refers to a thickness from 70 cm to 120 cm according to [28]. The prevailing ice thickness investigated in this paper is 80 cm and at the lower threshold of the referred thickness range.

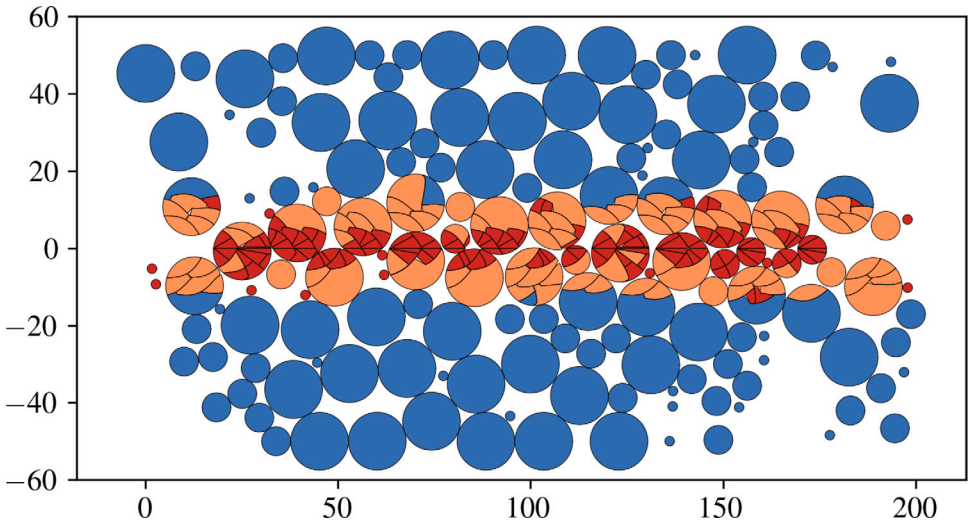

Fig. 1. Breaking pattern of floe-ice breaking simulation taken from [23, p. 48]. Measures on both axes are in m. Red floes are assumed to interact with the propeller, orange floes are pushed aside the ship and blue floes are not in contact with the ship's hull.

3. Floe-ice breaking simulation

The floe-ice breaking simulation is based on the further development of the work of Erceg [29], which is presented in detail by Sapp in [23]. This upgraded version extends the ice breaking of level ice to the more general breaking of ice floes of arbitrary size ranging from small ice floes to level ice. The breaking and interaction of the ship with ice floes is the governing scenario occurring in Antarctic water, where *S.A. Agulhas II* is operating. The setup of ship and ice floes is modelled in 2D with a parameterized third dimension.

The floe field used for this work is generated based on ice observation data from the Antarctic expedition of *S.A. Agulhas II* in 2019/20 on 18/12/2019, 20:20–20:30. The observation protocol contains averaged information about the floe diameter, the floe concentration and the floe thickness for time intervals of ten minutes. Based on these parameters, the floe fields are generated: First, the empty field is initialized by a predefined size (in this work: 200 m length, 110 m width). Second, the number of floes of different diameter ranges are computed and the corresponding number of floes based on the total ice concentration is placed randomly in the predefined floe field. The ice thickness of all floes is set to the averaged observed ice thickness. In the third step, the floe field is optimized to obtain an overlapping-free floe field. For a statistically representative result, the Monte Carlo method can be applied to multiple, randomly generated floe fields based on the same ice observation data.

Three main failure scenarios are regarded in the simulation: the floes can either fail by bending, by cracking or by direct rotation of the floes. The failure scenario is decided based on the size of the floe according to Lu [30].

For failure by bending, the ice floes are discretized in ice wedges with constant wedge angle as described in [31]. Failure by cracking starts with an initial crack orthogonal to the bow and, depending on the contact conditions and position of the floe along the bow, continues either orthogonal to the bow or tends to the failure pattern by bending. In both cases, the broken floes are checked again for their failure behaviour. All floes, that are sufficiently small according to [30], are not broken but assumed to fail by direct rotation.

To model the ship, different simple geometric parameters (length, beam, draught), as well as the bow shape and flare angles at the upper and lower ice waterline of the *S.A. Agulhas II* are used.

All floes in contact with the ship are failed by one of the scenarios described above and afterwards handled as pushed aside or pushed under the ship, depending on the size and the position of the floes. In this model it is considered that all floes pushed under the ship will end up in the propeller and contribute to the final load spectrum, which is considered being conservative.

Fig. 1 shows the broken ice floes computed by the presented simulation approach that are the basis for the FEM simulation of the propeller-ice interaction. The broken ice floes computed in this simulation are called *ice cusps* in the following to distinguish them from the non-broken ice floes.

4. Measurement of compressive strength of arctic ice

The development of the MCNS model [24] and further refinement with experiments [32] is based on the laboratory ice developed at the Hamburg University of Technology (TUHH). This ice is granular freshwater and in its properties significantly harder and stronger similar to glacier ice and it has the mission to generate conservative results. This also consequently means that it is of limited comparability to sea ice (especially summer sea ice) in which the *S.A. Agulhas II* is operating.

Fig. 2. Compressive load testing device.

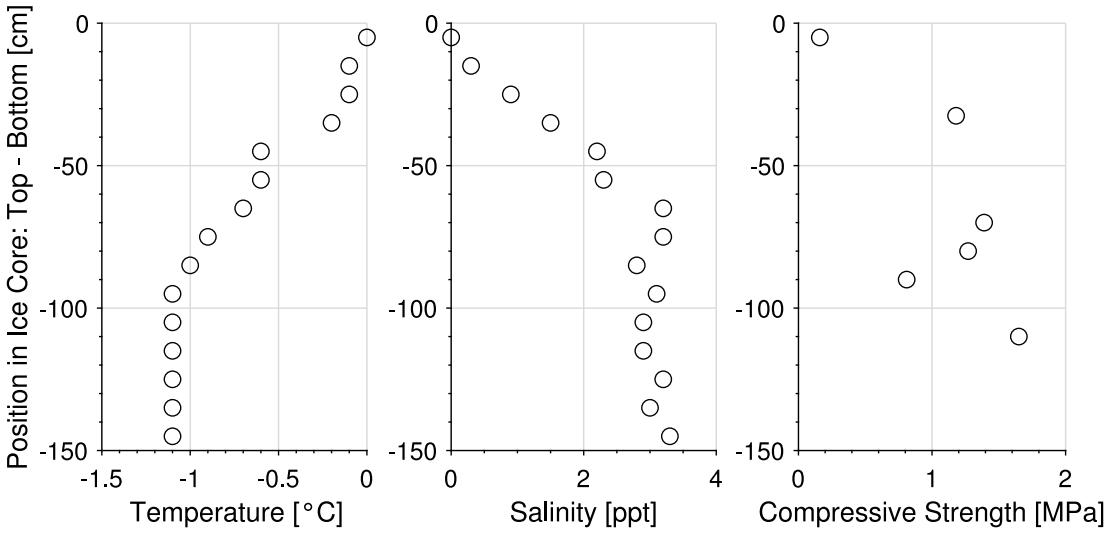

Fig. 3. Temperature, salinity and strength measurement results.

In order to modify the existing MCNS model reference measurements are conducted during an Arctic expedition to the North Pole in July 2023 [33]. The experiments are conducted with a portable device, which has a battery-driven hydraulic pump for a constant loading rate. The experimental setup is shown in Fig. 2. The ice specimen had a diameter of 9 cm which is the inner diameter of the core drill, a length of 10 cm and an average loading speed of 5 mm/s.

Based on the ice thickness of approx. 140 cm and the measured temperature and salinity profiles, it is considered to be first-year ice (Fig. 3). Fig. 3 shows also the conducted compressive strength measurements at the corresponding positions over thickness. The highest measured compression strength is 1.65 MPa.

The temperature of the ice for which this compressive failure stress was determined is around −1 °C. The compressive strength of sea ice strongly depends on the temperature as shown e.g. by Schulson [34, p. 246]. With higher temperatures that are closer to the melting point of ice, the compressive strength decreases to values of below 3 MPa [34, p. 244 ff]. The comparison with literature data supports the results of the measurements.

In order to change the existing MCNS model as conservatively as possible, the measurement with the highest compressive strength is selected from the existing data set of the expedition. The corresponding data set is shown in Fig. 3.

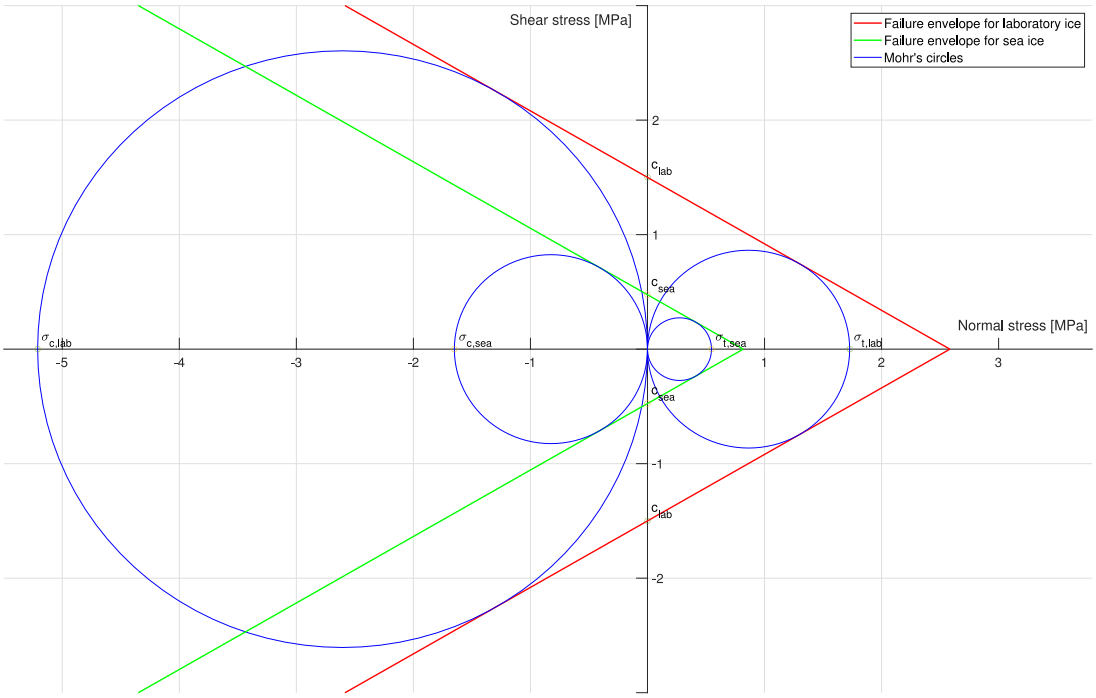

Fig. 4. Mohr–Coulomb compressive and tensile failure stress for the laboratory ice [36] and its adjusted properties for Arctic sea ice based on [33].

5. Computation of modified MCNS parameters for sea ice

The strength of the ice determines the loads acting on a ship propeller. The Mohr–Coulomb Nodal Split (MCNS) parameters that are proposed by Herrnring [24] have been developed for laboratory ice produced at the Hamburg University of Technology. This laboratory ice is designed to have properties that are as consistent as possible. To this end, the laboratory ice has a very low salt content and defects are avoided. Sea ice on the other hand has a high and varying content of salt and also a lot of defects. The data presented in Section 4 shows the varying compressive failure strength. Therefore, the material properties used to model the ice in the dynamic FEM simulation are modified to better fit the properties of sea ice. The highest measured compression strength presented in Section 4 is used as a basis for the computation of the modified MCNS parameters.

To explain the computation of the modified MCNS parameter, the MCNS method is briefly outlined here. Based on the Mohr-Coulumb hypothesis, the failure of a material can be described by two material parameters: the cohesion value c and the angle of friction ρ. In Fig. 4, four Mohr's circles are shown, the two larger circles corresponding to the original MCNS parameters developed for laboratory ice and the two smaller circles to the modified MCNS model introduced here for sea ice. On the right side of the y-axis, Mohr's circles are shown for ice that is exposed to uniaxial tensile stress. On the left side of the y-axis, Mohr's circle is shown for ice that is exposed to uniaxial compressive stress. If one of Mohr's circles touches the corresponding "failure envelope" (red line for original MCNS model and green line for modified MCNS model in Fig. 4), the material yields according to the Mohr–Coulomb material model. In Fig. 4, the cohesion value is the intersection between the y-axis and the green or red line. The angle of friction determines the slope of the failure envelope which can be expressed as $\tau = -\sigma \tan(\rho) + c$ [35, p. 49].

With these two variables, the tensile failure stress σ_t and the compressive failure stress σ_c of a Mohr–Coulomb material can be computed as [35, p. 50]

$$\sigma_t = 2c \frac{\cos(\rho)}{1 + \sin(\rho)} \tag{1}$$

$$\sigma_c = 2c \frac{\cos(\rho)}{1 - \sin(\rho)}. \tag{2}$$

As stated before, the highest compressive failure stress of 1.65 MPa in the measurements is used to determine the Mohr–Coulomb material parameters. The uniaxial compression failure stress for the laboratory developed by Herrnring is 5.23 MPa [24]. Under the assumption of an unchanged angle of friction, the cohesion value and the tensile failure stress are scaled linearly with the lower compressive failure stress as can be seen in Eqs. (1) and (2). This leads to the material parameters shown in Table 2 and Fig. 4.

With the Mohr–Coulomb approach, the plastic flow is initiated when Mohr's circle touches the failure envelope as shown in Fig. 4. From this point on, plastic flow occurs, and after a critical plastic strain ϵ_f of 0.2% is reached, the elements split at the element boundaries. The elements do not share the same global nodes and are connected at the nodes with a tied contact condition. The

Table 2
Original (based on laboratory ice) [24] and modified (based on sea ice) MCNS material parameters.

Variable	Original MCNS	Modified MCNS
elastic shear modulus G	3.5 GPa	3.5 GPa
Poisson's ratio ν	0.33	0.33
angle of friction ρ	0.526 rad	0.526 rad
cohesion value c	1.5 MPa	0.475 MPa
plastic failure strain ϵ_f	0.2%	0.2%
compressive failure stress σ_c	5.23 MPa	1.65 MPa
tensile failure stress σ_t	1.72 MPa	0.547 MPa

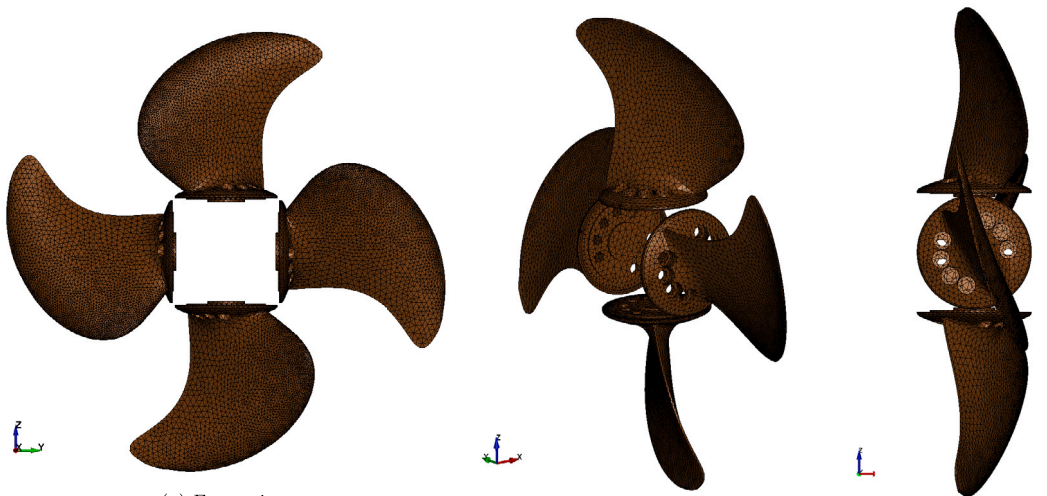

(a) Front view. (b) Angled view. (c) Side view.

Fig. 5. Mesh of the rigid propeller of the *S.A. Agulhas II*.

tied node contact condition is released if the critical plastic strain is reached. More details about the failure model can be found in [36, p. 67].

6. Numerical simulations of propeller-ice interaction

Different ice cusp geometries are exported from the floe-ice breaking simulation as planar polygons in combination with the thickness value of 0.8 m. The ice cusp geometries are imported into ANSYS to create a tetrahedral base mesh based on an automatic meshing approach using Delaunay triangulation. In the next step, the tetrahedral elements are exported to LS-Dyna and split into hexahedron elements. This meshing process is also outlined in [24, p. 021601-3]. The direct export of the ice cusps from the floe ice breaking simulation to the dynamic FEM simulation implies that the breaking or motion of the ice cusps under the ship is not considered.

To simulate the interaction between the propeller of the *S.A. Agulhas II* and the ice cusps computed in Section 3, the geometry of the four propeller blades is imported and meshed in ANSYS with tetrahedral elements. To reduce the computational effort the propeller is now modelled as rigid body with a rotation rate of $140\frac{1}{min}$. The propeller pitch $P_{0.7}^{95}$ is set to 4.9 m. This corresponds to a pitch percentage value of 95% of the maximum pitch of the *S.A. Agulhas II* (see Table 1). The pitch and rotation rate are chosen to match the values of the controllable pitch propeller that was set during the measurements presented later. The mesh of the propeller is shown in Fig. 5. The foot of the propeller is different from the actual propeller of the *S.A. Agulhas II*, but since the propeller-ice interaction is limited in the simulation to the higher diameters of the propeller, the effect of this on the results is negligible.

In addition to the rotational movement, the propeller moves forward with a translation velocity of $3\,\frac{\mathrm{m}}{\mathrm{s}}$ into the ice cusp. For every ice cusp, a separate simulation is performed. This neglects the interaction of the ice cusps with each other in the wake of the ship but enables a parallel simulation of the ice-propeller interaction for many ice cusps. At the beginning of the simulation, no forces act on the ice cusps and they are not moving. During the whole simulation, the ice cusps are not constrained by boundary conditions.

The interaction of the ship hull and rudder is at this point not integrated into the FEM simulation, even though this could be an improvement of the simulation for the future. The added mass effect is considered in the simulation which is why to the density of the ice ($900\,\frac{\mathrm{kg}}{\mathrm{m}^3}$) the density of water ($1000\,\frac{\mathrm{kg}}{\mathrm{m}^3}$) is added leading to a total density of the ice in the simulation of $1900\,\frac{\mathrm{kg}}{\mathrm{m}^3}$. Since the ice cusps are fully submerged, this approach is equivalent to adding the mass of the water displaced by the ice.

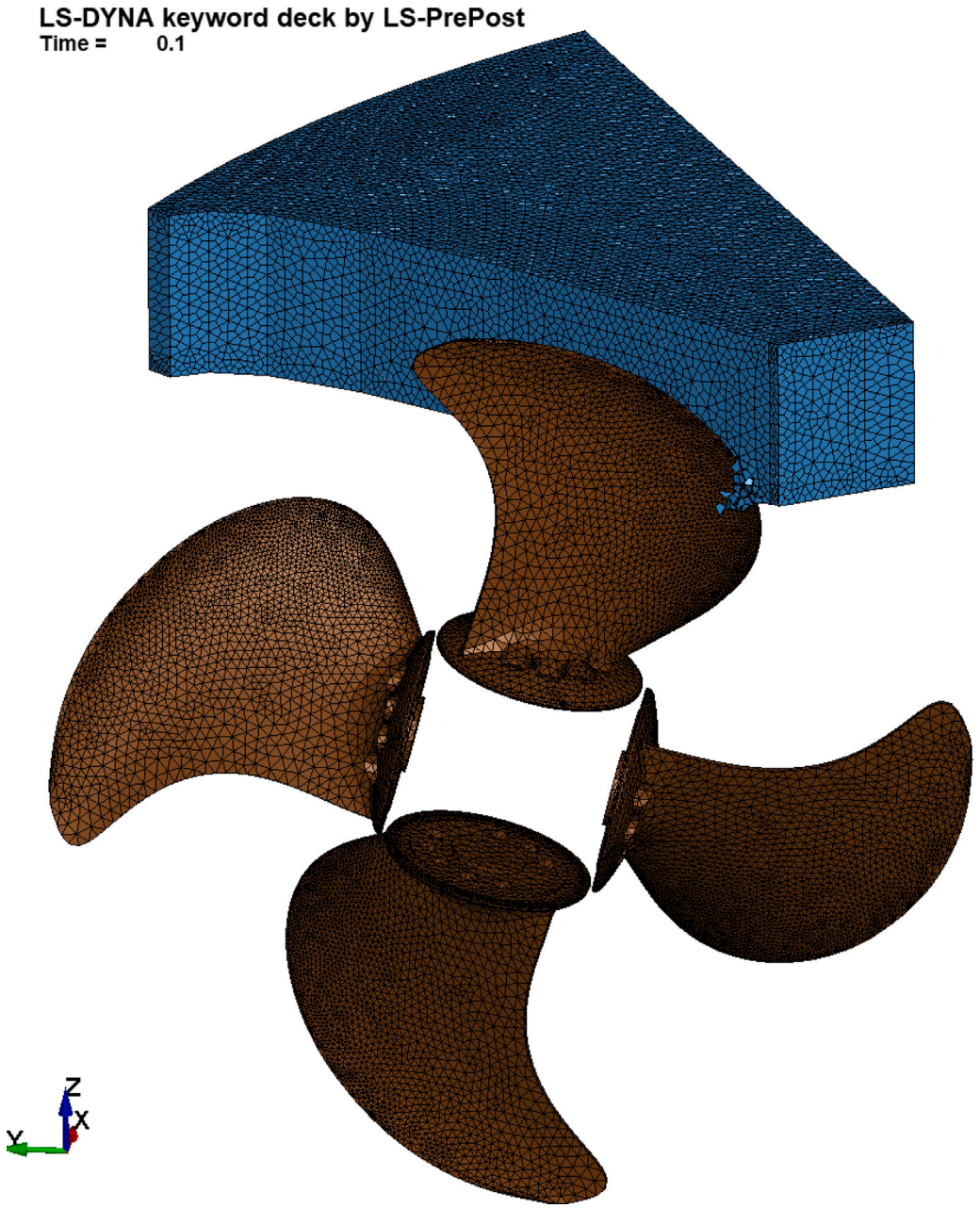

Fig. 6. Propeller mills through one of the ice cusps.

To consider the damping of the ice moving in water, Rayleigh damping is applied to ice elements with a mass-proportional damping factor of 0.5. This damping factor has been determined by a comparison of simulations with different damping factors and it prevents the ice cusp from being pushed too much forward with a high velocity by the propeller. The end time for the simulation is set such that the propeller mills through the whole ice cusps. However, some of the simulations end before the propeller has milled through the complete ice cusp since the ice cusp is flipped over or pushed away by the propeller.

The contacts between the propeller and the ice cusps as well as the different ice parts resulting from the crushing of the ice are a segment-based surface-to-surface contact [37, p. 11-87].

A challenging part remains the positioning of the ice when it is hit by the rotating propeller. Since the position of the ice cusps hitting the propeller is not known and has not been measured or recorded for the *S.A. Agulhas II*, the position of the ice cusps is estimated conservatively to be on the outer diameter of the propeller. The propeller rotates around the x-axis as visible in Fig. 6. The

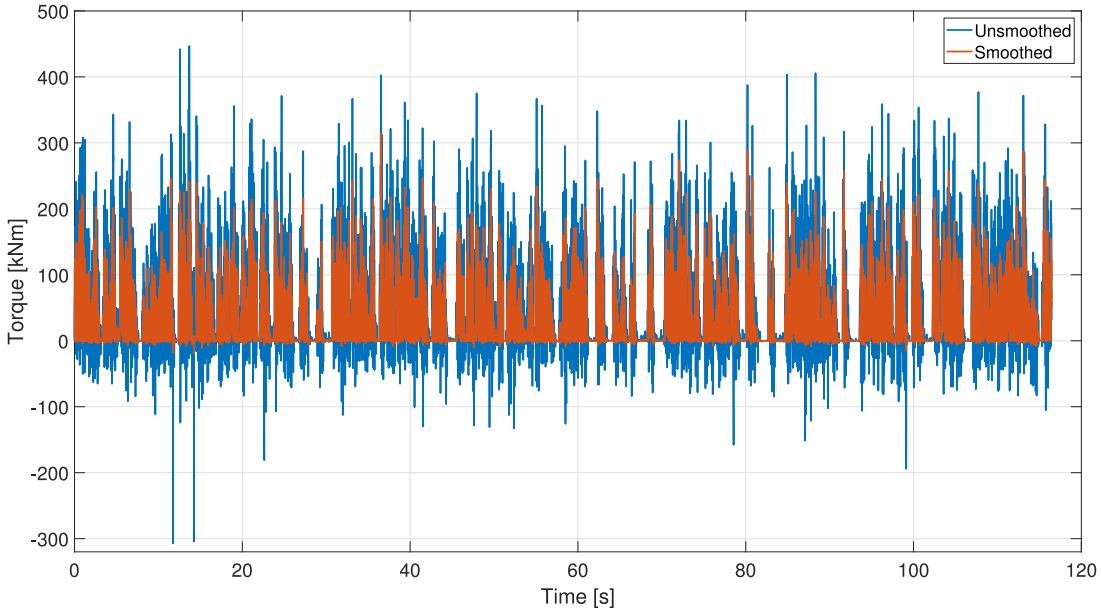

Fig. 7. Torque on the propeller axis computed in LS-Dyna in the milling scenario for the ice floes shown in Fig. 1.

centre of gravity of the ice cusp is placed in the x-z plane. The radius and accordingly also maximum z-coordinate of the propeller during rotation is 2.15 m.

The orientation of the ice cusps is unchanged from the floe ice-breaking simulation presented in Section 3. The polygon used for the generation of the prismatic shape of the ice cusp is parallel to the x-y plane. The lower and upper polygonal base areas of all ice cusps have a z-coordinate of 1.25 m and 2.05 m. This corresponds to propeller radius positions from 58% to 95%, where the 0.8 m thick ice is initially located. Since the ice is pushed upwards away from the propeller due to the multiple impacts with different blades, the positioning of the ice further up would lead to lower loads at later impacts. Therefore, this positioning is considered to generate the highest loads as the ice is hit on the highest possible radii.

In this paper, two different scenarios are considered. In the first scenario, the propeller moves forward in the x-direction and "mills" through the ice (see Fig. 5). This scenario is called the milling scenario.

In the second scenario, the propeller cuts through the centre of gravity of the ice and splits the ice cusp into 2 or more large pieces. This scenario is considered less likely compared to the first scenario since the ice would not be able to get into this position before being hit by the propeller. Despite this, it provides a much more conservative estimate of the loads that could act on the propeller. This scenario is called the central impact scenario. In both scenarios, the ice cusp has no initial velocity. A visualization of one of the propeller-ice interaction simulations for the milling scenario is shown in Fig. 6. To estimate the torque acting on the propeller shaft, the moment around the x-axis (coinciding with the rotation axis of the propeller) resulting from the propeller-ice contact condition is computed over the whole simulation.

In the first step, the simulation is conducted with the modified MCNS parameters for most of the ice cusps obtained in the floe-ice breaking simulation.

Only a set 100 randomly selected ice cusps of the 178 red ice cusps visible in Fig. 1 are simulated since the simulation of the whole set would excess the available computational resources on the High Performance Cluster (HPC) of the TUHH. The simulations are conducted over a time of several months with each simulation of an ice cusp using up to 16 CPUs for a maximum computation time of up to 500 h.

In Fig. 7, the torque computed with LS-Dyna is visualized as blue line over time by linking the results together. This unsmoothed torque has a maximum of 447 kNm at a time of 13.7 s. The propeller of the *S.A. Agulhas II* is made of stainless steel which is stiff but not rigid. Compared to the rigid propeller in the simulation, the moments and forces acting on the propeller shaft can therefore be assumed to be a bit smoother for full-scale measurements. The data is sampled in LS-Dyna with a sampling rate of 10 kHz while the measurement data is sampled with approximately 0.6 kHz. Since the torque data obtained from measurements on the *S.A. Agulhas II* is sampled with an approximately 17 times lower sampling rate, also the smoothed torque is visualized. The unsmoothed torque computed in LS-Dyna is smoothed by a moving average filter that has a window size of 17 and is therefore more suited for comparison with the measured signal sampled at the lower rate. The highest smoothed torque is 314 kNm at a time of 36.5 s.

In the second step, for one of the ice cusps, both scenarios are simulated once with the modified and once with the original MCNS model to analyse the impact of the modified MCNS parameters. Since the breaking patterns for the ice cusps are slightly

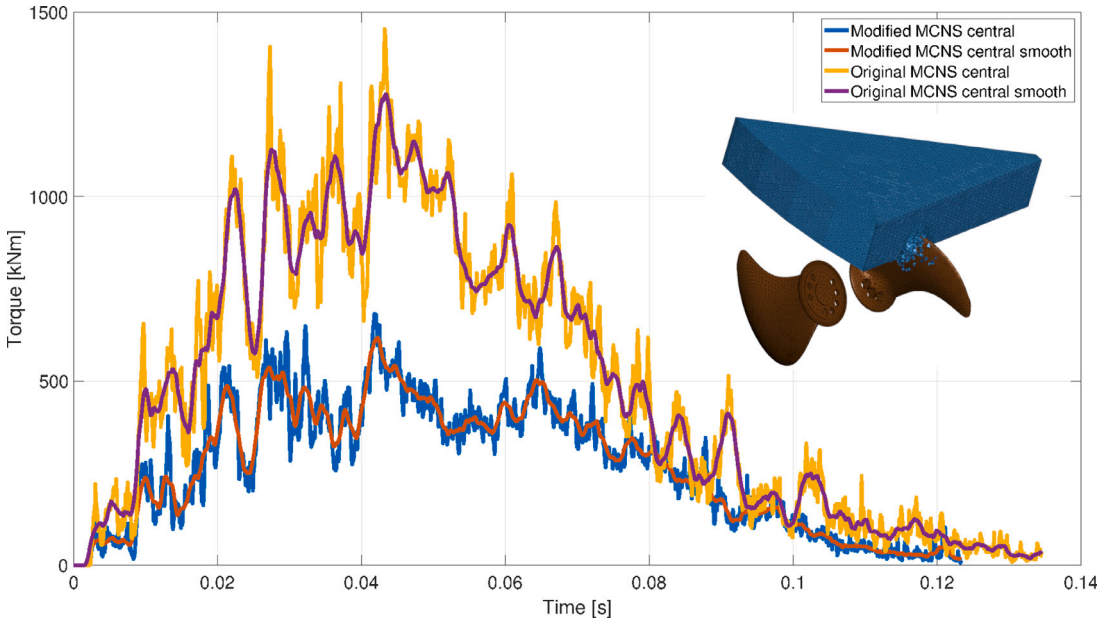

Fig. 8. Comparison of original and modified MCNS parameters for the central impact scenario.

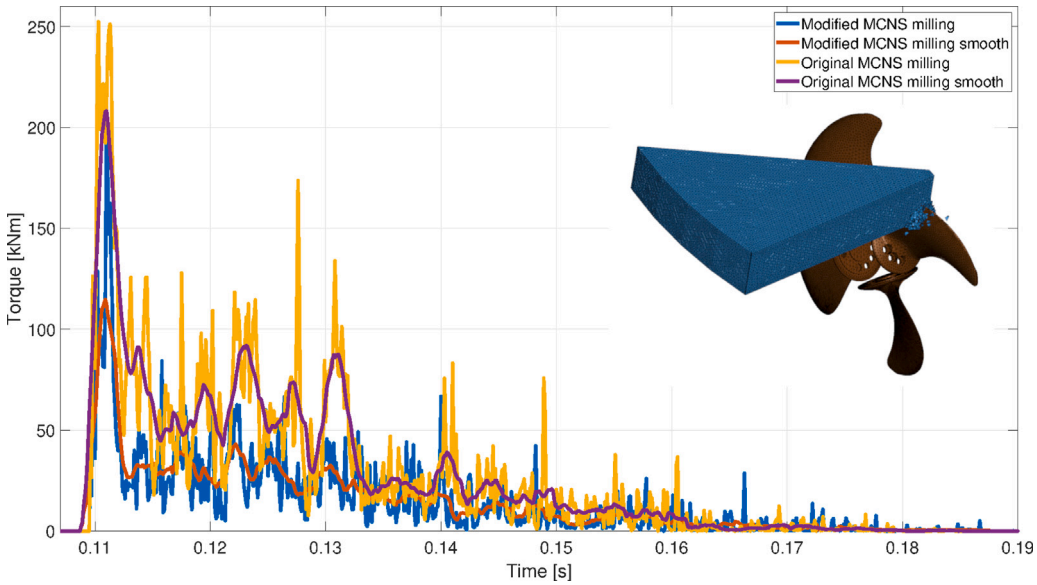

Fig. 9. Comparison of original and modified MCNS parameters for the milling scenario.

different between the simulation with the original and the modified MCNS model, the curves look similar but the peaks vary a little bit.

The resulting moments are shown in Fig. 8. and Fig. 9. The maximum peaks for the smoothed curves of the central impact scenario are 616 kNm for the modified MCNS model and 1278 kNm for the original MCNS model.

The maximum peaks for the smoothed curves of the milling scenario are 115 kNm for the modified MCNS model and 208 kNm for the original MCNS model. In the milling scenario, the ice cusp does in contrast to the central impact scenario not experience a global failure due to the contact with the first blade. The maximum peaks for the smoothed curves when the second blade hits the ice are 104 kNm for the modified MCNS model and 221 kNm for the original MCNS model. The impact of the blades leads to a rotation of the ice cusp that flips the ice cusp over on the sharp edge. This flipping effect is stronger for the original MCNS model since the contact forces are bigger for this model and the mass of the ice cusp is for both scenarios the same. Due to this effect, subsequent impacts cannot be properly compared.

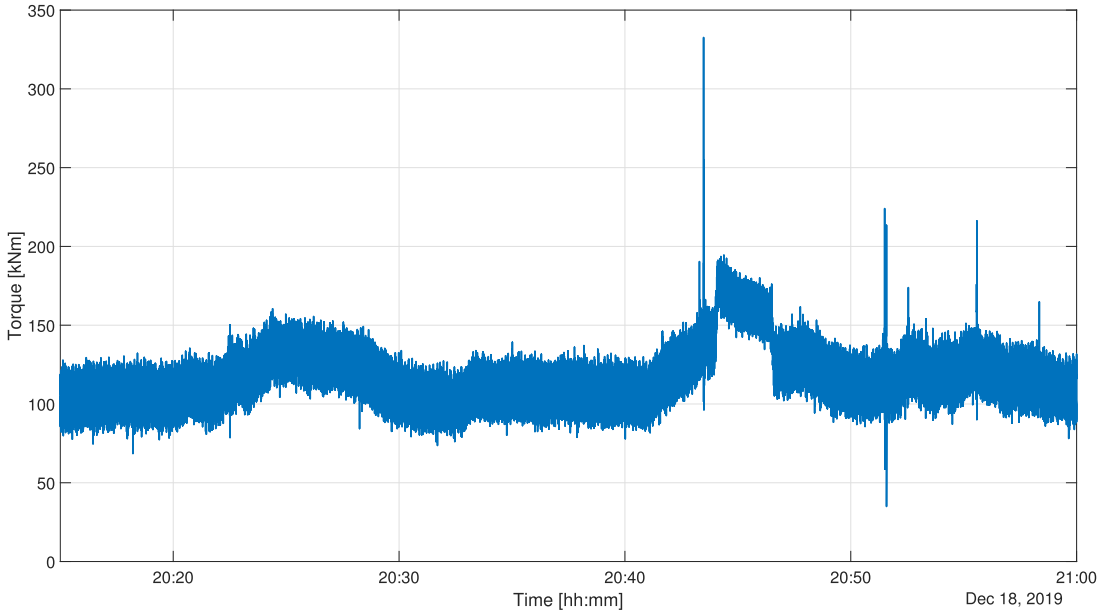

Fig. 10. Propeller torque data measured and computed on the *S.A. Agulhas II* [20].

The data suggest that the higher failure strength of the original MCNS model leads to a roughly two times higher moment on the propeller shaft.

7. Comparison to data from SA Agulhas II

In the last step, the torque and load spectrum estimated with LS-Dyna are compared with measurements conducted on the *S.A. Agulhas II*. Details about the measurements and computation of the torque on the propeller shaft of the *S.A. Agulhas II* can be found in Nickerson [38, p. 2 ff] and [20]. The torque is measured on the propeller shaft with a strain gauge bridge and the inverse model developed by Nickerson [20] is used to deduce the corresponding torque acting on the shaft at the propeller.

The torque at the propeller computed with this inverse model operating in ice conditions is shown in Fig. 10 for the interval 20:18 to 21:00 on December 19, 2019. The ice observation data used for the floe-ice breaking simulation presented in Section 3 and Fig. 1 are taken from this interval. This should enable a direct comparison of the torque data obtained with the presented framework to the torque data computed based on the measurements on the *S.A. Agulhas II*. The data in Fig. 10 is sampled with a frequency of 1 kHz and the mean value of the torque in 117 kNm. The torque on the propeller is strongly influenced by the water flow around the propeller, which is not considered in the simulation framework. To improve the comparability, the base torque acting on the propeller when no ice is present should be subtracted for later analysis. This base torque cannot be computed exactly from Fig. 10 but can be estimated to be around 100 kNm since this is the lowest value around which the torque oscillates. The three highest distinctive peaks show torque values of 333 kNm, 224 kNm and 216 kNm. Even though this set is too small to be statistically representative, it gives an impression of which torques are to be expected.

The dataset based on FEM simulations in LS-Dyna with the modified MCNS model (shown in Fig. 7) is compared with the torque obtained based on measurements on the *S.A. Agulhas II* [20] (shown in Fig. 10) in a histogram in Fig. 11. This histogram shows the probability density function of these two completely independent datasets. The dataset shown in Fig. 10 is modified for the probability density function such that both datasets have the same baseline. This is done by subtracting the base torque of 100 kNm from all data points visible in Fig. 10.

The comparison of all torques of the dataset shows an acceptable agreement in the lower range as the comparability in this region is limited due to variations in rotation rate, forward speed and pitch angle of the propeller in the measurements that are not considered in the simulation. In the range of the higher torques a significant overestimation of the torques computed in the LS-Dyna simulation is visible. This overestimation will be discussed in detail in the Discussion section.

Another insightful comparison is possible by only comparing the peak value visible in the simulations and in the measurement-based data. In Fig. 12, the maximum values for all 100 ice cusp simulations in LS-Dyna are visualized in a histogram for both the smoothed and the unsmoothed torques. The mean of the peak torques for the unsmoothed dataset is 289 kNm, and the mean for the smoothed dataset is 189 kNm. The distribution in the smoothed dataset resembles a Gaussian distribution and has its highest probability of 21% in the two intervals between the 175 kNm and 225 kNm. The distribution in the unsmoothed dataset does not show one distinctive maximum but four intervals of high probability between 250 kNm and 350 kNm.

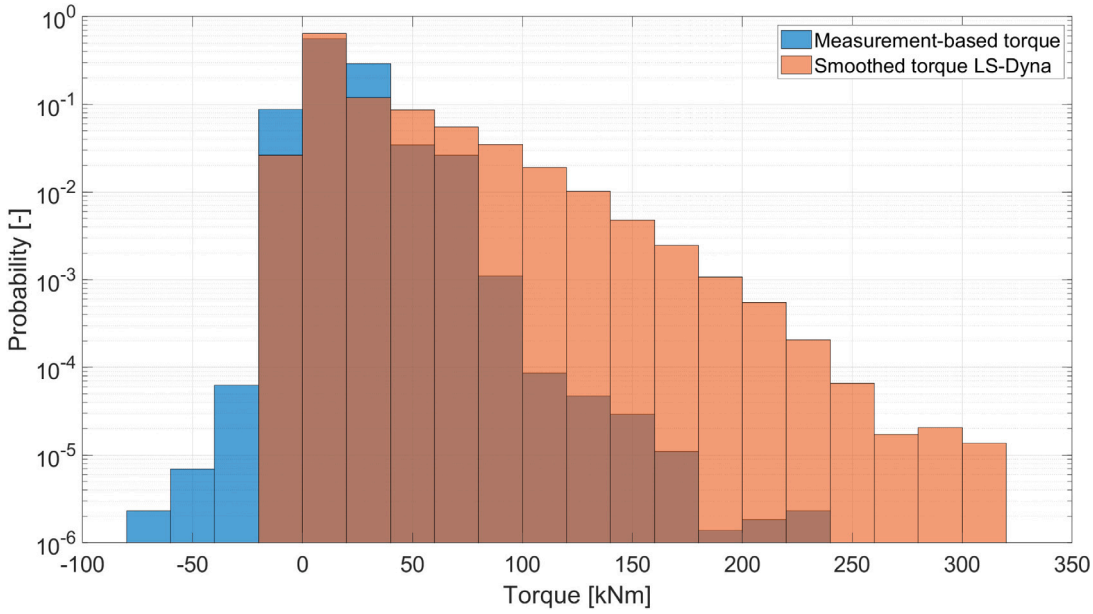

Fig. 11. Comparison of load spectrum for all torques computed based on *S.A. Agulhas II* measurements [20] shown in Fig. 10 and all torques simulated with the presented framework for the milling scenario as shown in Fig. 7. Ordinate has a logarithmic scale. Brown colour indicates overlap of both bars.

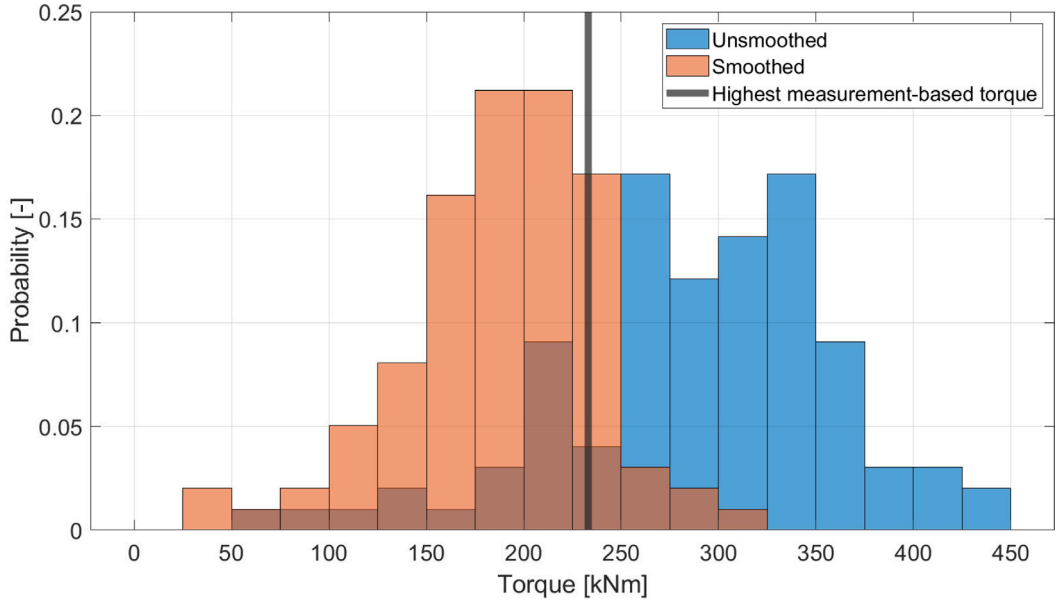

Fig. 12. Comparison of load spectrum for the peak torques of all 100 ice cusps simulated in LS-Dyna for the milling scenario for both torques lines shown in Fig. 7.

If the base torque of 100 kNm is subtracted from the measurement-based peak torques visible in Fig. 10, the three highest distinctive peaks have a torque value of 233 kNm, 124 kNm and 116 kNm. The highest peak of 233 kNm lies slightly above the two intervals with the smoothed dataset's highest probability (175 kNm–225 kNm) in Fig. 12. The remaining peaks show much smaller torques in intervals of lower probability.

In the last analysis of this section, the relation between the ice cusp volume and the induced maximal torques is examined. As shown in Fig. 13, the relation between the ice cusp volume and the maximal torque is slightly positive with a large scatter for both, smoothed and unsmoothed torque data. Consequently, the cusp volume has a certain impact on the torque, but other factors such as the relative position of the ice floe to the propeller blade play a role, too.

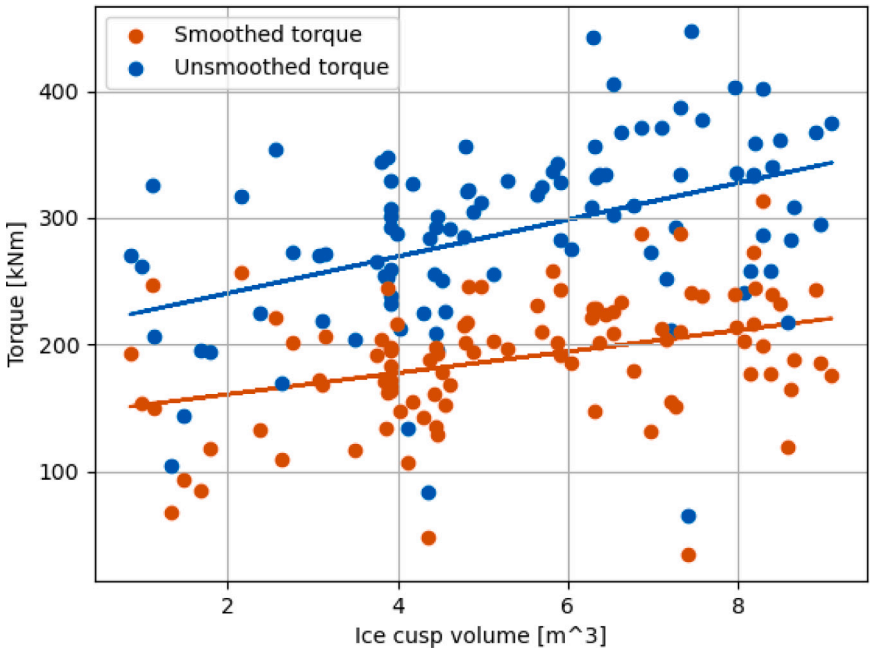

Fig. 13. Relation between the ice cusp volume and the maximal torque induces at the propeller.

8. Discussion

Concerning the computation of the modified MCNS parameters, some limitations are present. The compressive strength of the sea ice was conservatively estimated to be the highest strength measured in the Arctic Sea. A statistical evaluation of a larger dataset could here be useful to avoid an overestimation of the loads as visible in Fig. 11. The assumption of an unchanged angle of friction ρ is also not realistic but a computation of this angle would require tensile strength measurements. However, corresponding tensile strength measurements in the Arctic Sea are not available and of limited feasibility. A literature review reveals an angle of friction of sea ice between 0.56 rad and 0.8 rad [34, p. 290] or 0.7 rad and 0.91 rad [39]. This suggests that the angle of friction for sea ice might be higher compared to the laboratory ice manufactured at the TUHH. A higher angle of friction would lead to a lower tensile failure strength. A re-computation of the ice load spectrum for different angles of friction could be helpful here but would lead to an unfeasible high computation time.

A simulation with a flexible steel propeller could help obtain more accurate torque values at the propeller hub. The propeller has to be meshed (especially at the leading edge) with a sufficiently high mesh resolution to obtain realistic contact conditions. The small element size required for this would again increase the computational time in the simulation and make this approach (without additional formulations to reduce the computational time for small elements) computationally too expensive.

The assumption that all of the approximately 100 ice cusps are ending up in the propeller at a central position on the outer diameter is considered conservative, but not realistic. Underneath the hull, larger pieces might undergo additional breaking due to the interaction with the hull and acting pressures. Furthermore, the curved shape of the hull helps guide the ice pieces back to the side at the surface. In consequence, only a fraction of all submerged ice pieces end up in the propeller. These ice cusps would also show a rotational movement or a velocity component in the upward direction. Additionally, the interaction of several ice cusps in the vicinity of the propeller could lead to blocking effects. This however depends on particular sizes and the local ship shape as well as acting pressures and velocities. With reasonable computational effort, it is currently not possible to quantify the actual amount of ice that interacts with the propeller. In marine engineering, we rather prefer to be on the conservative side avoiding underestimating loads or load spectra. For this reason, the floes submerged are all accounted to the ice load spectrum, while acknowledging that the number of interactions might be over-estimated. The process of additional floe breaking between the bow and propeller while sliding along the hull cannot be assessed and is beyond the scope of this paper.

The analysis of the relationship between the ice cusp volume and the torque showed only a weak correlation, therefore the assumption of no further breaking of the ice cusps is consequently considered to be of reduced significance for the resulting load spectrum.

In the dataset based on measurements from the *S.A. Agulhas II*, it is not certain how many ice cusps hit the propeller since there is no recording of the ice below the ship. Furthermore, the dataset available from the *S.A. Agulhas II* evaluated here only covers a period of less than one hour, in which only a few distinctive peaks can be identified that could be attributed to significant contact of the propeller with large ice cusps. The simulated number of interactions in the LS-Dyna dataset is at least an order of magnitude

higher and in combination with the conservative assumptions in the simulation is believed to explain sufficiently well the difference at higher torques between the two datasets.

These observations can explain that the load spectrum computed with the presented simulation framework shows higher torques than the load spectrum based on the measured data from the *S.A. Agulhas II*.

Additional developments in the material model might also offer the potential to improve the simulation of the propeller-ice interaction. Such improvement could include the strain rate dependency on failure strength of ice as e. g. shown in experiments related to this research project. [32,40]. The ice material model could be also extended to include a more detailed fracture model such as the cohesive zone model instead of the simpler nodal splitting approach [41,42]. This model would also be better suitable to include the inhomogeneous and anisotropic nature of the ice grain sizes but would increase the computational time, which would severely limit the possible number of simulations for the presented setup. The disadvantage of the methods mentioned so far is that the crack can only occur along element boundaries or, in the case of the cohesive zone method, at the element boundaries, that are connected by cohesive elements. This effect leads to a strong mesh dependency of the crack path in these methods. Phase-field methods [43] or the extended finite element method (XFEM) [44] could allow for arbitrary crack paths but reach a limit due to the excessive mesh deformation if a structure such as ice splits into numerous smaller pieces that exhibit strong rotations in the simulation. Also, contact modelling of fractured surfaces is hard to realize with these methods. In the presented simulations, the small element sizes and the tetrahedral shape of the ice elements used in the presented simulation should be sufficient to allow for realistic crack propagation.

Despite its natural limitation due to the lack of data and information the agreement between the numerical simulations and the full-scale measurements are considered satisfying and the reproduction of the measurements with the presented framework is successful.

Finally, we want to compare the simulated and measured data with the design maximum torque in the Polar rules ([11, p. I3-5]). The maximum propeller ice torque, $Q_{\max}$, is applied to the propeller diameter, D, greater than a reference diameter, D_{limit}, $D \geq D_{\text{limit}}$ ([11, p. I3-5]) according to Eq. (3) with the ice class specific reference ice thickness $H_{\text{ice}} = 2$ m.

$$D_{\text{limit}} = 1.81 H_{\text{ice}} = 3.62 \text{ m} \tag{3}$$

The ice strength index $S_{\text{qice}} = 1.15$ for blade ice torque is taken from ([11, p. I3-3]). All other parameters used to calculate the maximum torque in Eq. (4) are found in Table 1.

$$Q_{\max} = 202\,(1 - d/D)\,S_{\text{qice}} {H_{\text{ice}}}^{1.1} \left(P_{0.7}/D\right)^{0.16} \left(t_{0.7}/D\right)^{0.6} (nD)^{0.17} D^{1.9} = 879 \text{ kNm} \tag{4}$$

In comparison to the measured and simulated data in Fig. 12, the design maximum torque for the *S.A. Agulhas II* is two to three times higher. However, it must be acknowledged that the simulated and measured ice thickness was rather at the lower threshold of the PC5 design conditions.

Nevertheless, the presented simulation framework is capable of computing the ice loads acting on a ship propeller and the complete breaking process of the ice in much more detail compared to other approaches.

9. Summary and conclusion

A framework for the simulation of the breaking of sea ice at the bow and the propeller of a ship is presented which is capable of accurately estimating the torque acting on a ship propeller. This framework reproduced measurements conducted on the polar research ship *S.A. Agulhas II*. An existing MCNS model developed for laboratory ice is modified based on measurements of the compressive strength of ice in the Arctic Sea. The resulting modification leads to an approximately three times lower compressive and tensile failure strength.

The framework simulates in the first step the breaking of ice floes at the bow of the ship. The resulting ice cusp shapes are then combined with the modified MCNS model to obtain realistic ice shapes and properties for the FEM simulation of the propeller-ice interaction. The ship parameters in the simulation framework are taken from the *S.A. Agulhas II*, but may be adapted to other ships. The properties of the original and modified MCNS model are compared for different propeller-ice interaction scenarios. This reveals that the lower failure strength of the ice modelled with the modified MCNS properties causes roughly two times lower torques at the propeller for the corresponding ice floe and propeller shape.

In the next step, the FEM simulation of the propeller-ice interaction is performed for the milling scenario with approximately 100 different ice cusp shapes obtained in the floe-ice breaking simulation. The resulting torque acting on the propeller is compared with the torque data obtained on the *S.A. Agulhas II*. The simulation results show a good agreement, despite several unknowns. In the comparison of the load spectra, the presented simulation frameworks overestimated the peak torques which can be attributed to the conservative assumptions made in the development of the framework as discussed in the previous section.

The presented framework is considered to have proven its functionality and concept. Even though the presented methodology is too complex and computationally expensive to be used directly for the design of a ship propeller operating in ice conditions, future developments will focus on improvement of the methods within the framework and increasing computational efficiency.

Nevertheless, the presented method is considered to contribute to a better understanding of the ice loads acting on a propeller and may assists in designing and operation in the future.

CRediT authorship contribution statement

Jorrid Lund: Writing – review & editing, Writing – original draft, Visualization, Validation, Software, Resources, Methodology, Investigation, Formal analysis, Data curation, Conceptualization. **Lina Sapp:** Writing – review & editing, Writing – original draft, Visualization, Software, Methodology, Investigation, Data curation. **Jan Manuel Kubiczek:** Validation, Methodology, Investigation, Data curation. **Angelo Mario Böhm:** Methodology, Conceptualization. **Franz von Bock und Polach:** Writing – review & editing, Writing – original draft, Supervision, Resources, Project administration, Methodology, Funding acquisition, Conceptualization.

Declaration of competing interest

The authors declare that they have no known competing financial interests or personal relationships that could have appeared to influence the work reported in this paper.

Acknowledgements

The authors would like to acknowledge support from:

- MarTERA - an ERA-NET Cofund scheme of Horizon 2020 of the European Commission - and the Research Council of Norway (Project No. 311502), the Federal Ministry for Economic Affairs and Climate Action of Germany (Project No. 03SX519B), and Department of Science and Technology of South Africa, through the HealthProp project
- The EU project ARICE (EU grant agreement No. 730965) Ships and Platforms of Opportunity Programme in cooperation with the company PONANT.

Data availability

Data will be made available on request.

References

[1] PAME. Arctic shipping status report #1. Tech. rep., Arctic Council; 2024, URL https://www.pame.is/projects/arctic-marine-shipping/arctic-shipping-status-reports.[Accessed 24 Jul 2024].
[2] Stkepień A, Arnarsson S, Dam KIM, Justus D, Latola K, Luszczuk M, et al. Strategic assessment of development of the Arctic: Assessment conducted for the European Union. Tech. rep., Arctic Centre, University of Lapland; 2014, URL https://www.arcticinfo.eu/images/pdf/SADA_report.pdf. [Accessed 24 Jul 2024].
[3] Council A. Arctic shipping update: 37% increase in ships in the arctic over 10 years. 2024, online [Accessed 24 Jul 2024].
[4] Boebel O. The expedition ps89 of the research vessel Polarstern to the WeddellSea in 2014/2015, vol. 689, Bremerhaven: Alfred Wegener Institute for Polar and Marine Research; 2015, http://dx.doi.org/10.2312/BzPM_0689_2015.
[5] Blenkey N. Polar star beats engineering challenges to complete mission. 2018, https://www.marinelog.com/news/video-polar-star-beats-engineering-challenges-to-complete-mission/. [Accessed 24 Jul 2024].
[6] Brigham L, Mccalla R, Cunningham E, Barr W, Vanderzaag D, Santos-Pedro V, et al. Arctic marine shipping assessment 2009 report. Tech. rep., Arctic Council; 2009, p. 194.
[7] Kim Y-H, Min S-K, Gillett NP, Notz D, Malinina E. Observationally-constrained projections of an ice-free arctic even under a low emission scenario. Nat Commun 2023;14. http://dx.doi.org/10.1038/s41467-023-38511-8.
[8] von Bock und Polach RUF, Klein M, Kubiczek J, Kellner L, Braun M, Herrnring H. State of the art and knowledge gaps on modelling structures in cold regions. In: Proceedings of the ASME 2019 38th international conference on ocean, offshore and arctic engineering. International conference on offshore mechanics and arctic engineering, vol. 8, Polar and Arctic Sciences and Technology; Petroleum Technology; 2019, http://dx.doi.org/10.1115/OMAE2019-95085, V008T07A014.
[9] Purcell E, Nejad A, Böhm AM, Sapp L, Lund J, Von Bock Und Polach F, et al. On methodology for a digital twin of ship propulsion under harsh environmental conditions. In: Proceedings of the ASME 2024 43rd international conference on ocean, offshore and arctic engineering. 2024.
[10] DNV. Rules for classification of ships - Part 6 additional class notations- Chapter 6 cold climate cold climate. 2023.
[11] IACS. Requirements concerning polar class. Int Assoc Classif Soc Lond 2011.
[12] Veitch B. Predictions of ice contact forces on a marine screw propeller during the propeller-ice cutting process. Helsinki University of Technology; 1995.
[13] Soininen H. A propeller-ice contact model. Helsinki University of Technology; 1998.
[14] Wang J. Prediction of propeller performance on a model podded propulsor in ice (propeller-ice interaction (Ph.D. thesis), Memorial University; 2007.
[15] Xiong WP, Wang C, Wang CH, Ma QW, Xu P. Analysis of shadowing effect of propeller-ice milling conditions with peridynamics. Ocean Eng 2020;195:106591. http://dx.doi.org/10.1016/J.OCEANENG.2019.106591.
[16] von Bock und Polach RUF, Molyneux D. Model ice: A review of its capacity and identification of knowledge gaps. In: Proceedings of the ASME 2012 36st international conference on ocean, offshore and arctic engineering. Proceedings of the ASME 2017 36th International Conference on Ocean, Offshore and Arctic Engineering, Trondheim; 2017, p. 9.
[17] von Bock und Polach RUF, Gralher S, Ettema R, Kellner L, Stender M. The non-linear behavior of aqueous model ice in downward flexure. Cold Reg Sci & Technol 2019. http://dx.doi.org/10.1016/J.COLDREGIONS.2019.05.001.
[18] Böhm AM, Sapp L, von Bock und Polach RUF. Derivation of a numerical propeller-ice interaction model. In: 8th international symposium on marine propulsors, smp 2024. Norwegian University of Science and Technology, Department of Marine Technology; 2024, p. 199–207. http://dx.doi.org/10.15480/882.9367.
[19] de Waal R, Bekker A, Heyns P. Data for indirect load case estimation of ice-induced moments from shaft line torque measurements. Data Brief 2018;19:1222–36. http://dx.doi.org/10.1016/j.dib.2018.05.115.
[20] Nickerson BM, Bekker A. Inverse model for the estimation of ice-induced propeller moments using modal superposition. Appl Math Model 2022;102:640–60. http://dx.doi.org/10.1016/j.apm.2021.10.005.

[21] Saleh A, Gilges M, Lehmann B, Jacobs G. Assessing the influence of the running-in phase in ship's stern tube bearings on wear development during ice collision loads. In: Detlefsen O, Olbert GA, Abdel-Maksoud M, editors. Proccedings of the eighth international symposium on marine propulsors 2024 (smp'24). Berlin: University Library (TUB) of Hamburg University of Technology (TUHH),Hamburg University of Technology AND Port Said University; 2024, p. 171–80. http://dx.doi.org/10.15480/882.9318.
[22] Amin M, Veitch B. Application of polar class rules for fatigue to an existing arctic class icebreaker propeller. In: Proceedings of the fifth international symposium on marine propulsors. 2017, p. 1–8.
[23] Sapp L. Development of a Floe-Ice Breaking Simulation for the Generation of Propeller–Ice Load Spectra. 2023, http://dx.doi.org/10.15480/882.8574.
[24] Herrnring H, Ehlers S. A finite element model for compressive ice loads based on a Mohr-Coulomb material and the node splitting technique. J Offshore Mech Arct Eng 2021;144(2):021601. http://dx.doi.org/10.1115/1.4052746.
[25] Böhm AM, Herrnring H, von Bock und Polach F. Splitting-tests of laboratory-made granular ice with a propeller-like indenter. In: International conference on offshore mechanics and arctic engineering, vol. 85918, American Society of Mechanical Engineers; 2022, http://dx.doi.org/10.1115/OMAE2022-78186, V006T07A013.
[26] Müller F, Böhm AM, Herrnring H, von Bock und Polach RUF, Ehlers S. Experimental and numerical analysis of ice crushing tests with different shaped ice specimens. In: International conference on offshore mechanics and arctic engineering, vol. 86885, American Society of Mechanical Engineers; 2023, V006T07A015.
[27] Yoon S, Herrnring H, Müller F, von Bock und Polach F. Numerical analysis of ice blocks impact on stiffened plates according to a Mohr-Coulomb material and node splitting technique. In: International conference on offshore mechanics and arctic engineering, vol. 86885, American Society of Mechanical Engineers; 2023, V006T07A013.
[28] WMO. Sea ice nomenclature. 2014, URL https://library.wmo.int/idurl/4/41953. [Accessed 24 Jul 2024].
[29] Erceg S, Erceg B, von Bock und Polach F, Ehlers S. A simulation approach for local ice loads on ship structures in level ice. Mar Struct 2022;81:103117. http://dx.doi.org/10.1016/j.marstruc.2021.103117.
[30] Lu W, Lubbad R, Løset S, Kashafutdinov M. Fracture of an ice floe: Local out-of-plane flexural failures versus global in-plane splitting failure. Cold Reg Sci & Technol 2016;123:1–13. http://dx.doi.org/10.1016/j.coldregions.2015.11.010.
[31] Nevel DE. The narrow free infinite wedge on an elastic foundation. Tech. rep., Cold Regions Research and Engineering Laboratory (US),U.S. Army Snow Ice and Permafrost Research Establishment, Corps of Engineers; 1961.
[32] Böhm AM, Herrnring H, von Bock und Polach F. Data from uniaxial compressive testing of laboratory-made granular ice. Data Brief 2022;42:108236. http://dx.doi.org/10.1016/J.DIB.2022.108236.
[33] von Albedyll L, Kubiczek JM, von Bock und Polach F, Haas C. Sea ice thickness, ice loads, and navigability during the North Pole cruise CC110823 of Le Commandant Charcot in August 2023. Cruise report. Tech. rep., ARICE,Alfred Wegener Institute, Helmholtz Centre for Polar and Marine Research; 2024, URL https://epic.awi.de/id/eprint/58238/. [Accessed 24 Jul 2024].
[34] Schulson EM, Duval P. Creep and Fracture of Ice. Cambridge University Press; 2009, http://dx.doi.org/10.1017/cbo9780511581397.
[35] Gross D, Seelig T. Bruchmechanik : Mit einer einführung in die mikromechanik, 6. Aufl. 2016. SpringerLink bücher, Berlin, Heidelberg: Springer Vieweg; 2016, http://dx.doi.org/10.1007/978-3-662-46737-4.
[36] Herrnring HJ. Experimental and numerical investigation of brittle ice crushing loads (Ph.D. thesis), Hamburg University of Technology; 2023, http://dx.doi.org/10.15480/882.4923.
[37] LS-Dyna. Keyword user's manual R13. Southpointe: Livermore Software Technology (LST), An Nsys Company; 2021.
[38] Nickerson BM, Bekker A. Recommendations for regularization in the inverse estimation of ice-induced propeller moments for ice-going vessels. Cold Reg Sci & Technol 2021;192:103378. http://dx.doi.org/10.1016/j.coldregions.2021.103378.
[39] Ringeisen D, Hutter N, von Albedyll L. Deformation lines in arctic sea ice: intersection angle distribution and mechanical properties. Cryosphere 2023;17(9):4047–61. http://dx.doi.org/10.5194/tc-17-4047-2023.
[40] Böhm AM, Müller F, Herrnring H, Von Bock und Polach RU. High-speed impact drop tower tests of cylindrical granular ice specimens. In: Proceedings of the 27th international conference on port and ocean engineering under arctic conditions (POAC 2023). 2023.
[41] Kellner L, Lu W, Ehlers S, Høyland K. Study on the cohesive edge crack in a square plate with the cohesive element method. Int J Fract 2020. http://dx.doi.org/10.1007/s10704-021-00560-9.
[42] Kellner L. Analyzing the complexity of ice with explainable machine learning for the development of an ice material model [Ph.D. thesis], Hamburg University of Technology; 2022, http://dx.doi.org/10.15480/882.4076.
[43] Francfort GA, Marigo J-J. Revisiting brittle fracture as an energy minimization problem. J Mech Phys Solids 1998;46(8):1319–42. http://dx.doi.org/10.1016/s0022-5096(98)00034-9.
[44] Moes N, Dolbow J, Belytschko T. A finite element method for crack growth without remeshing. Internat J Numer Methods Engrg 1999;46:131–50. http://dx.doi.org/10.1002/(SICI)1097-0207(19990910)46:13.0.CO;2-J.